Near-Field Tomography without Phase Retrieval

P. Scott Carney, Vadim A. Markel, and John C. Schotland
Department of Electrical Engineering, Washington University, St. Louis, Missouri 63130
(Received 11 December 2000)

We investigate the near-field inverse scattering problem with evanescent waves. An analytic solution to this problem within the weak-scattering approximation is used to show that the usual Rayleigh limit may be overcome even when measurements are made without phase information. Applications to a novel form of three-dimensional microscopy with subwavelength resolution are described.

DOI: 10.1103/PhysRevLett.86.5874 PACS numbers: 42.30.Wb, 42.25.Fx, 42.30.Rx

There has been considerable recent interest in the development of methods which extend the spatial resolution of optical microscopy beyond the classical diffraction limit. Researches in near-field optics have provided a powerful set of experimental approaches to directly address this problem [1]. These approaches, which include near-field scanning optical microscopy and total internal reflection microscopy, have been used to obtain subwavelength-resolved maps of the optical intensity near surfaces of effectively two-dimensional systems. However, when the sample presents manifestly three-dimensional structure, interpretation of the resultant images has proven to be problematic [2]. In recent months, significant progress towards the development of three-dimensional near-field imaging has been made on two fronts. Nanotomography, a destructive method in which a sample is successively eroded and then imaged layer by layer with a scanning probe microscope was reported in Ref. [3]. A *nondestructive* approach has also been suggested and is based upon the solution to the linearized near-field inverse scattering problem for three-dimensional inhomogeneous media [4]. For this latter method, the input data for the image reconstruction algorithm depend on the amplitude and phase of the scattered field. Measurements of the optical phase, particularly in the near field, are notoriously difficult since detectors generally record only intensities, necessitating the use of a holographic measurement scheme.

In this Letter we present the theoretical foundations for three-dimensional near-field microscopy which achieves subwavelength resolution without retrieval of the optical phase. The proposed method, to which we refer as near-field tomography, obtains from an analysis of the inverse scattering problem in which the incident field consists of a coherent superposition of evanescent waves. The superoscillatory properties of such waves may be used to encode structure on subwavelength scales. Our results are remarkable in three regards. First, we circumvent the near-field phase problem by employing measurements of the power extinguished from the probe fields. Second, the fields on which the power measurements are performed may be monitored far from the scatterer and thus subwavelength resolution is obtained from far zone measurements. Third, by developing an analytic approach to the inverse problem in the form of an explicit inversion formula, we produce an image reconstruction algorithm which is strikingly robust in the presence of noise. Computer simulations are used to illustrate our approach in model systems.

We begin by considering an experiment in which a monochromatic field is incident on a dielectric medium with susceptibility $\eta(\boldsymbol{r})$. For simplicity, we ignore the effects of polarization and consider the case of a scalar field $U(\boldsymbol{r})$ which obeys the reduced wave equation

$$\nabla^2 U(\boldsymbol{r}) + k_0^2 U(\boldsymbol{r}) = -4\pi k_0^2 \eta(\boldsymbol{r}) U(\boldsymbol{r}), \qquad (1)$$

where k_0 is the free space wave number. The incident field will be taken to consist of a superposition of two evanescent waves (see Fig. 1)

$$U^{(i)}(\boldsymbol{r}) = a_1 e^{i\mathbf{k}_1\cdot\boldsymbol{r}} + a_2 e^{i\mathbf{k}_2\cdot\boldsymbol{r}}, \qquad (2)$$

with amplitudes a_1 and a_2. Here the complex wave vectors $\mathbf{k}_1$ and $\mathbf{k}_2$ are of the form $\mathbf{k}_j = (\boldsymbol{q}_j, k_z(\boldsymbol{q}_j))$ with transverse part $\boldsymbol{q}_j$ and $k_z(\boldsymbol{q}_j) = i(q_j^2 - k_0^2)^{1/2}$ for $j = 1, 2$. If the evanescent waves are generated by a prism of refractive index n then $k_0 \le |\boldsymbol{q}_j| \le nk_0$. By monitoring the change in the power content of the totally reflected waves due to the presence of the scatterer, we may obtain the power lost by the probe fields, the extinguished power. In a sense, the interference of these waves leads to a form of holography carried out *within* the scattering medium. The power extinguished from the incident beams may be obtained from a generalization of the optical theorem [5] and is given by the expression

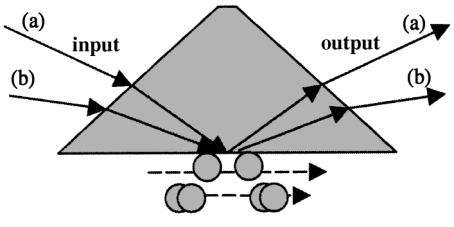

FIG. 1. Illustrating the experiment. Beams (*a*) and (*b*) generate evanescent waves which are incident on the scatter. The extinguished power is then measured at the output via difference measurements with and without the scatterer present.

 0031-9007/01/86(26)/5874(4)$15.00

$$P(a_1, a_2) = \frac{4\pi}{k_0} \operatorname{Im}[|a_1|^2 A(\mathbf{k}_1^*, \mathbf{k}_1) + a_1^* a_2 A(\mathbf{k}_1^*, \mathbf{k}_2) + a_2^* a_1 A(\mathbf{k}_2^*, \mathbf{k}_1) + |a_2|^2 A(\mathbf{k}_2^*, \mathbf{k}_2)], \tag{3}$$

where $A(\mathbf{k}_1, \mathbf{k}_2)$ is the scattering amplitude associated with the scattering of a plane wave with wave vector $\mathbf{k}_1$ into a plane wave with wave vector $\mathbf{k}_2$. It will prove useful to extract the cross terms from (3), that is to gain information about the scattering amplitude for nonzero momentum transfer. This can be accomplished for any set of $\mathbf{k}_1$ and $\mathbf{k}_2$ through four measurements of the extinguished power where the relative phases are varied between measurements. To this end we define the following data function [5,6]:

$$D(\mathbf{k}_1, \mathbf{k}_2) = \frac{k_0}{8\pi a_1^* a_2} \{P(a_1, ia_2) - P(a_1, -ia_2) + i[P(a_1, a_2) - P(a_1, -a_2)]\}. \tag{4}$$

It may be seen from (3) that the data function is related to the scattering amplitude by

$$D(\mathbf{k}_1, \mathbf{k}_2) = A(\mathbf{k}_1^*, \mathbf{k}_2) - A^*(\mathbf{k}_2^*, \mathbf{k}_1). \tag{5}$$

The data function uniquely determines $\eta(\boldsymbol{r})$ as may be seen from the analytic properties of the scattering amplitude. It should be stressed that this result is independent of any approximations beyond the use of a scalar model.

We now address the inverse problem. We restrict our attention to the weak-scattering approximation. Accordingly, the scattering amplitude may be calculated perturbatively to lowest order in η with the result

$$A(\mathbf{k}_1, \mathbf{k}_2) = k_0^2 \int d^3 r\, e^{-i(\mathbf{k}_1 - \mathbf{k}_2)\cdot \boldsymbol{r}} \eta(\boldsymbol{r}). \tag{6}$$

Noting that the wave vectors $\mathbf{k}_1$ and $\mathbf{k}_2$ may be specified by their transverse parts alone, it may be found that

$$D(\boldsymbol{q}_1, \boldsymbol{q}_2) = 2ik_0^2 \int d^3 r \exp\{-i(\boldsymbol{q}_1 - \boldsymbol{q}_2)\cdot \boldsymbol{\rho} - i[k_z^*(\boldsymbol{q}_1) - k_z(\boldsymbol{q}_2)]z\}\alpha(\boldsymbol{r}), \tag{7}$$

where $\boldsymbol{r} = (\boldsymbol{\rho}, z)$ with $\boldsymbol{\rho}$ the transverse spatial coordinate, $\alpha(\boldsymbol{r}) \equiv \operatorname{Im}\eta(\boldsymbol{r})$ is the absorptive part of the susceptibility, and the dependence of D on $\boldsymbol{q}_1$ and $\boldsymbol{q}_2$ has been made explicit.

We assume that $D(\boldsymbol{q}_1, \boldsymbol{q}_2)$ is known for $(\boldsymbol{q}_1, \boldsymbol{q}_2)$ in the data set $\mathcal{Q}$ and introduce a function $\chi(\boldsymbol{q}_1, \boldsymbol{q}_2)$ which is unity if $(\boldsymbol{q}_1, \boldsymbol{q}_2) \in \mathcal{Q}$ and is zero otherwise. For convenience, we introduce the function $\Phi(\boldsymbol{q}, \boldsymbol{Q}) = D(\boldsymbol{q}, \boldsymbol{Q} + \boldsymbol{q})\chi(\boldsymbol{q}, \boldsymbol{Q} + \boldsymbol{q})/2ik_0^2$ where $\boldsymbol{q}, \boldsymbol{Q}$ range over all space. Making use of these definitions, we arrive at the system of equations

$$\Phi(\boldsymbol{q}, \boldsymbol{Q}) = \int_0^L dz\, K(\boldsymbol{q}, z; \boldsymbol{Q})\tilde{\alpha}(\boldsymbol{Q}, z), \tag{8}$$

where

$$K(\boldsymbol{q}, z; \boldsymbol{Q}) = \exp\{i[k_z(\boldsymbol{Q} + \boldsymbol{q}) - k_z^*(\boldsymbol{q})]z\}\chi(\boldsymbol{q}, \boldsymbol{Q} + \boldsymbol{q}), \tag{9}$$

$\tilde{\alpha}(\boldsymbol{Q}, z) = \int d^2\boldsymbol{\rho} \exp(i\boldsymbol{Q}\cdot\boldsymbol{\rho})\alpha(\boldsymbol{r})$, and L is the range of $\alpha(\boldsymbol{r})$ in the z direction. For fixed $\boldsymbol{Q}$, Eq. (8) defines a one-dimensional integral equation for $\tilde{\alpha}(\boldsymbol{Q}, z)$ whose pseudoinverse solution has the form

$$\tilde{\alpha}(\boldsymbol{Q}, z) = \int d^2\boldsymbol{q}\, d^2\boldsymbol{q}'\, K^*(\boldsymbol{q}, z; \boldsymbol{Q}) \times \langle \boldsymbol{q}|M^{-1}(\boldsymbol{Q})|\boldsymbol{q}'\rangle \Phi(\boldsymbol{q}', \boldsymbol{Q}), \tag{10}$$

where the matrix element $\langle \boldsymbol{q}|M^{-1}(\boldsymbol{Q})|\boldsymbol{q}'\rangle$ is obtained from the overlap integral

$$\langle \boldsymbol{q}|M(\boldsymbol{Q})|\boldsymbol{q}'\rangle = \int_0^L dz\, K(\boldsymbol{q}, z; \boldsymbol{Q})K^*(\boldsymbol{q}', z; \boldsymbol{Q}). \tag{11}$$

It may be verified by direct substitution that (10) satisfies (8). Finally, we apply the inverse Fourier transform in the transverse direction and note that we may restrict the integrations over $\boldsymbol{Q}$ to $|\boldsymbol{Q}| \le 2nk_0$ and $\boldsymbol{q}, \boldsymbol{q}'$ to $\mathcal{Q}_1$ with $\mathcal{Q}_1 = \{\boldsymbol{q}_1 : (\boldsymbol{q}_1, \boldsymbol{q}_2) \in \mathcal{Q}\}$ to arrive at our main result:

$$\alpha(\boldsymbol{r}) = \frac{1}{2i(2\pi)^2 k_0^2} \int_{|\boldsymbol{Q}|\le 2nk_0} d^2\boldsymbol{Q}\, e^{-i\boldsymbol{Q}\cdot\boldsymbol{\rho}} \int_{\mathcal{Q}_1\times\mathcal{Q}_1} d^2\boldsymbol{q}\, d^2\boldsymbol{q}'\, K^*(\boldsymbol{q}, z; \boldsymbol{Q}) \langle \boldsymbol{q}|M^{-1}(\boldsymbol{Q})|\boldsymbol{q}'\rangle \chi(\boldsymbol{q}', \boldsymbol{Q} + \boldsymbol{q}')D(\boldsymbol{q}', \boldsymbol{Q} + \boldsymbol{q}') \tag{12}$$

which is the required inversion formula.

The solution we have constructed to the inverse problem is the unique minimum L^2 norm solution of (7). This statement follows from the fact that (12) may be interpreted as the singular value decomposition (SVD) [7] of the pseudoinverse solution to (7). A detailed discussion of the analytic SVD of the linear integral operator defined by (7) is beyond the scope of this Letter and will be presented elsewhere. Nevertheless, it is important to appreciate that the SVD provides a natural means of regularization of the inverse problem which sets the resolution of the reconstructed image to be commensurate with the available data. In particular, we regularize $M^{-1}(\boldsymbol{Q})$ by setting

$$\langle \boldsymbol{q}|M^{-1}(\boldsymbol{Q})|\boldsymbol{q}'\rangle = \sum_\ell R[\sigma_\ell(\boldsymbol{Q})] \frac{\langle \boldsymbol{q}|c_\ell(\boldsymbol{Q})\rangle \langle c_\ell(\boldsymbol{Q})|\boldsymbol{q}'\rangle}{\sigma_\ell^2(\boldsymbol{Q})}, \tag{13}$$

where the $|c_\ell(\boldsymbol{Q})\rangle$ are eigenfunctions of $M(\boldsymbol{Q})$ with eigenvalues $\sigma_\ell^2(\boldsymbol{Q})$. Here $R(\sigma)$ filters the small eigenvalues, the simplest choice being a cutoff whereby R is set to zero below some fixed threshold. Alternatively, Tikhonov regularization, Wiener filtering, or other methods may be employed.

To demonstrate the feasibility of the inversion, we have numerically simulated the reconstruction of $\alpha(\boldsymbol{r})$ for a collection of spherical scatterers. The forward data were calculated by considering the scattering of evanescent waves from a homogeneous sphere including multiple scattering terms by means of a partial wave expansion. We consider a sphere of radius a centered at the point $(0, 0, a)$ with refractive index n, n being related to the scattering potential by the expression $n^2 = 1 + 4\pi\eta$. It may be found that

$$A(\mathbf{k}_1, \mathbf{k}_2) = e^{ia\hat{\mathbf{z}}\cdot(\mathbf{k}_1 - \mathbf{k}_2)} \sum_{\ell=0}^{\infty} (2\ell + 1) A_\ell P_\ell(\hat{\mathbf{k}}_1 \cdot \hat{\mathbf{k}}_2), \tag{14}$$

where A_ℓ are the usual partial wave expansion coefficients [8] and P_ℓ are the Legendre polynomials. Since we consider evanescent waves, the argument of the Legendre polynomials in (14) may exceed unity. The series may nonetheless be shown to be convergent due to the rapid decay of the A_ℓ with increasing ℓ.

The forward data were obtained for a collection of six spheres of radius $\lambda/20$ and index of refraction $n = 1.1 + 0.2i$, distributed on three planes as shown in Fig. 2. All scatterers are present simultaneously in the forward simulation with intersphere scattering neglected. The set $\mathcal{Q}$ of transverse wave vectors was taken to consist of all wave vectors $\boldsymbol{q}_{1,2}$ corresponding to evanescent waves attainable with a prism of index n such that $|\boldsymbol{q}_{1x}| \le nk_0$, $|\boldsymbol{q}_{1y}| \le k_0/2$, $\boldsymbol{q}_2 = \boldsymbol{Q} + \boldsymbol{q}_1$, and the physical requirement that $k_0 \le |\boldsymbol{q}_{1,2}| \le nk_0$ is always imposed. When $\mathcal{Q}$ consists of discrete points, the integrals in (12) become sums. More specifically, integration over $\boldsymbol{q}, \boldsymbol{q}'$ was performed on a rectangular grid with lattice spacing Δq and over $\boldsymbol{Q}$ on a rectangular grid with lattice spacing ΔQ. Regularization was achieved by setting $R(\sigma) = \Theta(\sigma - \sigma_c)$ where the cutoff $\sigma_c = \epsilon \max[\sigma_\ell(\boldsymbol{Q})]$ with scale factor ϵ.

In Fig. 2 we present simulations of experiments done with two different prisms, one with index of refraction $n = 5$, the other with $n = 10$ (as might be encountered in the infrared). We show the reconstructions obtained at depths of 0.05λ, and 0.25λ which correspond to the two separate equatorial planes of the original distribution of scatterers. The relevant parameters were taken to be $\Delta q = k_0/2$, and $\Delta Q = k_0/4$ for the $n = 10$ prism. For the $n = 5$ case we took $\Delta q = k_0/4$, and $\Delta Q = k_0/8$. The regularization parameter ϵ was taken to be $\epsilon = 10^{-3}$ for the $z = 0.05\lambda$ layer and $\epsilon = 10^{-2}$ for the $z = 0.25\lambda$ layer. Complex Gaussian noise of zero mean was added to the data function at various levels as indicated.

In principle the inversion formula (12) provides an exact reconstruction of the scatterer when the data function is known for all possible transverse wave vectors. In practice, however, the resolution of the reconstruction is controlled by several factors including the index of the prism, the depth of the slice, and choice of regularization parameters. These effects may be understood by observing that the resolution is governed by the low pass filtering ($|\boldsymbol{Q}| \le 2nk_0$) that is inherent in the transverse Fourier integral in (12) and additionally by the exponential decay of high-frequency components of the scattered field with increasing degree of evanescence. In general, with a prism of index n the transverse resolution will be on the order of $\lambda/2n$ at a depth of $\lambda/2n$ after which it falls off linearly. This is seen in the $n = 10$ simulations where the spheres whose edges are separated by $\lambda/20$ may be resolved in the slice at a depth of $\lambda/20$. However, the spheres in the next layer at $\lambda/4$ with the same spacing are not resolvable,

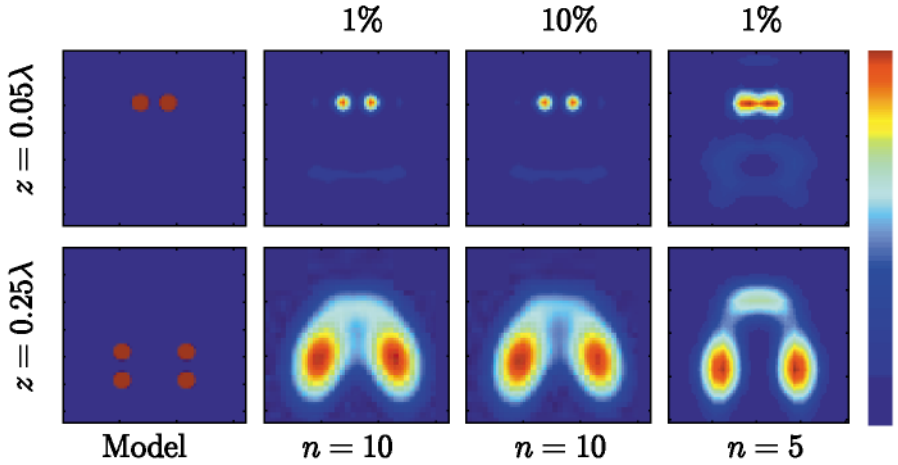

FIG. 2 (color). The simulated tomographs. The field of view is $\lambda \times \lambda$ in each image. The scatterers used in the forward simulation are shown in the column labeled "Model." The percentages given across the top indicate the noise level compared to the signal level. The indices listed across the bottom indicate the index of refraction of the prism needed to generate the waves used in the simulations. Each reconstruction was normalized by its maximum value and imaged using the linear color scale shown to the right.

but the groups of spheres which are spaced at $\lambda/4$ may be resolved. For the $n = 5$ case the scatterers in the top layer are not well resolved, but the scatterers in the deeper layer are well resolved. That in these simulations the lower index prism seems to produce better images of the deeper layer may be attributed to the fact that we make use of a fixed number of wave vectors, so that the reconstructions involving the lower index prism take into account a greater number of lower spatial frequency waves which probe the deeper layers.

It may be observed that the reconstruction algorithm is very robust in the presence of noise. This may be attributed to the fact that the inverse problem is overdetermined. More specifically, the parametrization of the data function by $(\boldsymbol{q}_1, \boldsymbol{q}_2)$ is four dimensional while the absorption is parametrized by the three-dimensional position vector $\boldsymbol{r}$. When the data are known for a finite set of discrete points this underlying degeneracy manifests itself as a discrepancy between the number of singular functions in the regularized inversion kernel and the number of data points, the latter being greater than the former. This has the effect of performing a weighted average over groups of data points, each group being associated with a particular singular function. Since the data function is produced by taking differences between power extinction measurements, it is expected that regardless of other statistical properties of the noise it will be of zero mean. Thus the averaging process enhances the signal.

In conclusion, we have shown that it is possible to reconstruct the three-dimensional subwavelength structure of a scattering medium from power extinction measurements. Several comments on our results are necessary. First, the improved resolution is made possible by the use of evanescent waves as illumination so that we may directly probe the high spatial frequency structure of the scatterer. Second, we have obtained a solution to the linearized near-field inverse scattering problem without measurement of the optical phase. Third, our approach provides an analytic solution rather than a numerical solution to the inverse problem. Finally, our results are of general physical interest since they are applicable to the inverse scattering problem with any scalar wave using data derived from power extinction measurements.

[1] D. Courjon and C. Bainier, Rep. Prog. Phys. **57**, 989 (1994); C. Girard and A. Dereux, Rep. Prog. Phys. **59**, 657 (1996).

[2] D. Van Labeke and D. Barchiesi, J. Opt. Soc. Am. A **9**, 732 (1992); R. Carminati and J. Greffet, Opt. Commun. **116**, 316 (1995); J. Opt. Soc. Am. A **12**, 2716 (1995).

[3] R. Magerle, Phys. Rev. Lett. **85**, 2749 (2000).

[4] P. S. Carney and J. C. Schotland, Appl. Phys. Lett. **77**, 2798 (2000).

[5] P. S. Carney, J. Mod. Opt. **46**, 891 (1999).

[6] P. S. Carney, E. Wolf, and G. S. Agarwal, J. Opt. Soc. Am. A **11**, 2643 (2000).

[7] F. Natterer, *The Mathematics of Computerized Tomography* (Wiley, New York, 1986), Chap. 4.

[8] The coefficient A_ℓ is given by the expression $A_\ell = i\beta_\ell/[k_0(\beta_\ell - i\gamma_\ell)]$ with $\beta_\ell = j_\ell(nk_0a)j'_\ell(k_0a) - nj'_\ell(nk_0a) \times j_\ell(k_0a)$ and $\gamma_\ell = nj'_\ell(nk_0a)n_\ell(k_0a) - j_\ell(nk_0a)n'_\ell(k_0a)$.